Detection and characterization of red blood cell (RBC) aggregation with photoacoustics

Eno Hysi[a], Ratan K. Saha[a,b], Min Rui[a] and Michael C. Kolios[a*]
[a]Department of Physics, Ryerson University, Toronto, Canada;
[b]Applied Material Science Division, Saha Institute of Nuclear Physics, Kolkata, India

ABSTRACT

Red blood cells (RBCs) aggregate in the presence of increased plasma fibrinogen and low shear forces during blood flow. RBC aggregation has been observed in deep vein thrombosis, sepsis and diabetes. We propose using photoacoustics (PA) as a non-invasive imaging modality to detect RBC aggregation. The theoretical and experimental feasibility of PA for detecting and characterizing aggregation was assessed. A simulation study was performed to generate PA signals from non-aggregated and aggregated RBCs using a frequency domain approach and to study the PA signals' dependence on hematocrit and aggregate size. The effect of the finite bandwidth nature of transducers on the PA power spectra was also investigated. Experimental confirmation of theoretical results was conducted using porcine RBC samples exposed to 1064 nm optical wavelength using the Imagio Small Animal PA imaging system (Seno Medical Instruments, Inc., San Antonio, TX). Aggregation was induced with Dextran-70 (Sigma-Aldrich, St. Louis, MO) and the effect of hematocrit and aggregation level was investigated. The theoretical and experimental PA signal amplitude increased linearly with increasing hematocrit. The theoretical dominant frequency content of PA signals shifted towards lower frequencies (<30 MHz) and 9 dB enhancements in spectral power were observed as the size of aggregates increased compared to non-aggregating RBCs. Calibration of the PA spectra with the transducer response obtained from a 200 nm gold film was performed to remove system dependencies. Analysis of the spectral parameters from the calibrated spectra suggested that PA can assess the degree of aggregation at multiple hematocrit and aggregation levels.

Keywords: Red blood cell aggregation, photoacoustics, frequency-domain analysis

1. INTRODUCTION

Individual red blood cells (RBCs) have the tendency to form reversible aggregates which lead to the formation of 3D clusters known as rouleaux. It is known from experimental observations that RBC aggregation in whole blood is associated with the elevated concentration of plasma macromolecules such as fibrinogen and globulins[1]. Several studies have explored the use of fibrinogen mimicking macromolecules such as various molecular weight Dextrans as well as other polymers for inducing RBC aggregation[2]. RBC aggregation is a dynamic process since it depends upon a balance between the forces of aggregation (due to the adsorption and bridging of the macromolecules) and the forces of disaggregation (due to the electrostatic repulsion between adjacent cell surfaces)[3]. The process is also governed by the shear forces of blood flow. In stationary whole blood or in whole blood at low shear rates, RBCs aggregate to form rouleaux. However, at high shear rates the rouleaux are disrupted. Virtually no aggregation is observed in human blood for shear rates greater than 50/s[4]. The aggregation level thus plays an important role in blood flow, particularly in the microvascular system. Aggregation increases blood viscosity and affects the passage of cells through micro vessels, especially in venules with low shear flow[5]. Increased RBC aggregation has been observed in a variety of circulatory related diseases such as diabetes[6], thrombosis[7], myocardial infarction[8] and sepsis[9].

All available clinical techniques used for assessing RBC aggregation require the invasive withdrawal of blood. The most widely used clinical method for assessing RBC aggregation is the erythrocyte sedimentation rate which measures the sedimentation speed of a RBC sample[1]. Optical aggregometry techniques measure the intensity of backscattered or transmitted light through a RBC sample under shearing conditions to provide an assessment of the degree of aggregation during several time points of the aggregation process[8]. However, the indexes of aggregation provided by these methods

*mkolios@ryerson.ca

Photons Plus Ultrasound: Imaging and Sensing 2012, edited by Alexander A. Oraevsky, Lihong V. Wang,
Proc. of SPIE Vol. 8223, 82233E · © 2012 SPIE · CCC code: 1605-7422/12/$18 · doi: 10.1117/12.908685

may not directly relate to *in-vivo* conditions of RBC aggregation. Recently, several *in-vitro* experimental techniques were developed for characterizing aggregation but they either use ionizing radiation[10] or are not feasible for non-invasive assessment due to poor penetration depth[11]. Ultrasound (US) backscattering techniques currently represent the standard imaging tool for the non-invasive detection and characterization of RBC aggregation[12]. We propose the use of photoacoustics (PA) as a tool for the detection and assessment of RBC aggregation. PA is a non-invasive imaging modality which detects the optically induced acoustic waves produced from the transient thermoelastic expansion that occurs when the incident optical energy is absorbed[13]. The advantage of this hybrid technique lies in the fact that the scattering of the generated sound waves is two to three orders of magnitude smaller than optical waves thus allowing for greater imaging penetration due to smaller attenuation[14]. Due to the oxygen dependent optical absorption of blood, PA has been applied for mapping the oxygen saturation of normal and abnormal vasculature[15] in addition to imaging carcinomas using gold nanoparticles for enhanced contrast[16].

In a recent report by our group, we utilized frequency-domain analysis of the PA imaging data for characterizing RBC aggregation in human blood samples[17]. This approach is adopted from US analysis methods where the spectral characterization of the backscattered radiofrequency (RF) signals has been developed for quantitative tissue characterization[18] and therapy response monitoring[19]. The motivation for this analysis method is the fact that both US and PA images are typically constructed from the amplitude of the RF signals detected by the transducer thus rendering the results system dependent. By normalizing the experimental frequency-domain spectra from a region of interest (ROI) with the frequency response of the US transducer, a quasi-linear spectrum over the usable frequency bandwidth is obtained. A set of three parameters (slope, intercept and midband fit) can be extracted by performing linear regression on the normalized frequency spectrum[18]. In US tissue characterization, the spectral slope is an indicator of the effective scatterer shape and size and an increase in slope corresponds to a decrease in effective scatterer size. Similarly, the midband fit (defined as the value of the linear fit evaluated at the midpoint of the usable transducer bandwidth) is a measure of US backscatter and depends on the scatterer size, shape, acoustic impedance and concentration[20]. To date, frequency-domain analysis of PA imaging data has only been applied for assessing prostate adenocarcinoma tumours in a murine model[21] as well for detecting abnormal vasculature[22]. It is reasonable to expect that the PA frequency-domain spectra contain similar information about the size and concentration of the optical absorbers that are RBCs.

We present a theoretical and experimental approach based on the frequency-domain analysis of the PA RF signals for detecting and quantifying RBC aggregation. The theoretical model is based on the single particle approach and generates PA pressure fields from a collection of individual or clusters of spherical absorbers representing non-aggregating (NA) and aggregating (AG) RBCs, respectively. In practice however, transducers used for detecting PA signals have a finite bandwidth which consequently filters out many of the frequency components of the PA signals produced. The effect of the finite nature of the acoustic transducer receive bandwidth was also investigated. PA spectral analysis was then used to differentiate and characterize the aggregation level of RBCs. Porcine blood was used as an aggregation model to validate theoretical findings. PA spectral parameters from calibrated PA spectra were computed for various hematocrit and aggregation levels and were used as a tool to differentiate between NA and AG RBCs as well as different aggregation levels.

2. METHODS

2.1 Theoretical model and simulation methods

The theoretical model and the simulation methods used in this study were described in detail at a recent publication by our group[23,28]. This model simulated two-dimensional RBC configurations under NA and AG conditions. In this model, the finite nature of the transducer bandwidth was not taken into account. This was done in order to observe all the frequencies produced from samples of NA and AG RBCs. Coordinates of NA RBCs (modeled as homogenous spheres) were generated by employing a Monte Carlo method known as random sequential adsorption technique with the restriction that they would not overlap with existing particles under periodic boundary conditions. The RBCs were packed to form a compact aggregate using a hexagonal packing scheme. Aggregates were then randomly and repeatedly placed within the ROI to simulate a blood sample with AG RBCs. The PA signals from such a collection of RBCs were simulated by extending a theoretical model used by Diebold[24] based on the frequency-domain calculation of the PA pressure field generated by a spherical source uniformly irradiated by a laser with a delta function heating pulse. The PA

pressure with all the frequencies produced from the uniform irradiation of a single spherical absorber at a distance r in the surrounding medium can be written as

$$p_{\text{single}}(\hat{q}) = \frac{A v_s a^2}{r} \times \frac{\left[\sin\hat{q} - \hat{q}\cos\hat{q}\right]\exp(ik_f(r-a))}{\hat{q}^2\left[(1-\hat{\rho})(\sin\hat{q}/\hat{q}) - \cos\hat{q} + i\hat{\rho}\hat{v}\sin\hat{q}\right]}, \tag{1}$$

with

$$A = \frac{i\mu\beta I_0}{C_P}, \tag{2}$$

where, μ is the optical absorption coefficient, β is the isobaric thermal expansion coefficient, C_P is the heat capacity per unit mass for the spherically absorbing region and I_0 is the intensity of the optical radiation. The dimensionless frequency $\hat{q}$ is defined as $\hat{q} = \varpi a / v_s$ and a is the radius of the absorbing sphere. Here, ϖ is the intensity modulation frequency of the optical radiation. The dimensionless variables $\hat{\rho} = \rho_s / \rho_f$ and $\hat{v} = v_s / v_f$ represent the ratios of the density and the speed of sound, respectively. The subscripts s and f denote the spherical absorber and the surrounding fluid medium, respectively. Similarly, k_f is the wave number for the fluid medium related to the frequency by $k_f = \varpi / v_f$. For a collection of N absorbing spheres, the PA pressure field can be written as the linear superposition of the spherical waves emitted by the individual sources

$$p_{collection}(\hat{q}) = A v_s a^2 \times \frac{\left[\sin\hat{q} - \hat{q}\cos\hat{q}\right]}{\hat{q}^2\left[(1-\hat{\rho})(\sin\hat{q}/\hat{q}) - \cos\hat{q} + i\hat{\rho}\hat{v}\sin\hat{q}\right]} \times \sum_{n=1}^{N} \frac{\exp(ik_f(|\vec{r} - \vec{r}_n| - a))}{|\vec{r} - \vec{r}_n|}, \tag{3}$$

where, $\vec{r}_n$ is the position vector of the n^{th} particle. For each sample, 250 complex PA signals were computed from 250 configurations (NA or AG) by computing the inverse Fourier transform of equation (3). The simulation parameters used to evaluate equation (3) are summarized in table 1.

Table 1: The physical parameters used in the simulation. The parameters used to evaluate equation (2) are all set to 1 as they simply control the amplitude of the PA signal and not the frequency content.

ROI	$200 \times 200\,\mu m^2$	a	$2.75\,\mu m$
ρ_s	$1092\ kgm^{-3}$	β	$1\ K^{-1}$
ρ_f	$1005\ kgm^{-3}$	C_P	$1\ Jkg^{-1}K^{-1}$
v_s	$1639\ ms^{-1}$	μ	$1\ m^{-1}$
v_f	$1498\ ms^{-1}$	I_0	$1\ Jm^{-2}$

The effect of hematocrit on NA RBCs and aggregate size of AG RBCs was investigated. Three hematocrit levels (10, 20 and 40%) were simulated for the NA case. For the AG case, the degree of aggregation was assessed by the radius of gyration (R_g). The radius of gyration is the average squared distance of any point in the object from its center of mass. In this model, the radius was computed for a sphere and using the parallel axis theorem was extended to a collection of spheres representing an aggregate. In the AG case, three aggregation levels were constructed at 40% hematocrit for three radii of gyrations, 2, 10 and 15 μm. Here, a radius of gyration of 2 μm represents the NA case used to compare with the other aggregation levels.

2.2 Modeling finite bandwidth transducers

The finite nature of the transducer bandwidth was incorporated into the model by introducing a Gaussian function to the frequency domain solution of the wave equation, as shown in equation (3). By modeling a transducer with a finite bandwidth, the non band-limited PA spectra computed using equation (3) will be filtered by the response of the

transducer. The modeling of a finite bandwidth transducer can be accomplished by using a Gaussian function which is typically used to represent the frequency response profile of a transducer used for US[25] and PA measurements. The band-limited PA pressure from a collection of RBCs (NA and AG) was then written as

$$p_{collection}(\hat{q}) = Av_s a^2 \times \exp\left[-\frac{(\varpi-\varpi_0)^2}{2\sigma^2}\right] \times \frac{\left[\sin\hat{q}-\hat{q}\cos\hat{q}\right]}{\hat{q}^2\left[(1-\hat{\rho})(\sin\hat{q}/\hat{q})-\cos\hat{q}+i\hat{\rho}\hat{v}\sin\hat{q}\right]} \times \sum_{n=1}^{N}\frac{\exp(ik_f(|\vec{r}-\vec{r}_n|-a))}{|\vec{r}-\vec{r}_n|}, \quad (4)$$

where, ϖ_0 is the center frequency of the transducer and σ is related to the -6 dB bandwidth of the transducer. In this study, three transducers with 5, 15 and 55 MHz center frequency (-6 dB bandwidth of 60%) were used to filter the PA signals obtained from the non band-limited case for NA and AG RBCs at the same hematocrit and aggregation levels.

2.3 Blood samples

Fresh porcine blood was extracted from the femoral vein of Yorkshire pigs (Comparative Research, Toronto, ON) into spray-coated potassium EDTA vacutaners (Becton, Dickinson and Company, Franklin Lakes, NJ). The blood was centrifuged (1400 g for 6 minutes) to separate the plasma from the RBCs. The buffy coat containing the white blood cells was carefully removed and discarded. Isotonic phosphate buffered saline (PBS) was used to wash the remaining RBCs twice. Various hematocrit levels (10, 20 and 40%) were achieved by re-suspending the RBCs with PBS. Aggregation was induced by using Dextran-70 (molecular weight 70 kDa) (Sigma-Aldrich, St. Louis, MO). To achieve various degrees of aggregation, solutions of 1, 3 and 8% (wt/vol) concentration of Dextran-PBS ([Dextran-PBS]) were used to re-suspend NA RBCs at each hematocrit level. All experiments were completed within 4 hours of blood withdrawal.

2.4 Transducer response measurement

In order to obtain the frequency-domain response of the transducer used in this measurement, a gold film was deposited on a thin glass microscope cover slide with no annealing. The film had a thickness of 200 ± 5 nm and an area of ~0.25 cm^2. The gold film was used because it has a broad PA spectrum (and a flat response in the known bandwidth of the transducer) thus it can provide a good measurement of the transducer response in a PA passive mode. The laser was fired onto the film by emitting 4 pulses at each location while raster scanning the entire area of the film. A total of 20 PA signals were recorded from the gold film. The average power spectrum of 20 measurements was used as the response of the transducer for calibrating the power spectra from NA and AG RBCs and extracting the spectral parameters described above.

2.5 PA measurements and signal analysis

All PA measurements were conducted using the Imagio Small Animal PA imaging system (Seno Medical Instruments Inc., San Antonio, TX). The system consisted of a Q-switched Nd:YAG laser emitting 6 ns pulses with 10 Hz repetition rate and a wavelength of 1064 nm. The beam diameter was 9 mm and each pulse had an energy fluence of 2.5 mW/cm^2. The ultrasound transducer consisted of a 4 channel annular array centered at 5 MHz (-6 dB bandwidth: 2-8 MHz, focus: 29.5 mm) mounted coaxially to the laser. The RBC samples were loaded into a tygon tubes (Norton Performance Plastic, Akron, OH) with 0.05 cm inner diameter and 0.1 cm outer diameter which served as the sample holder. A vertical raster scan was performed with the laser emitting 4 pulses at each location (which were averaged to generate 1 RF line) within the vertical ROI covering the entire sample holder. A total of 20 PA signals were recorded for each solution, corresponding to a total of 100 laser pulses exposing each RBC sample.

For each scan, the PA signal amplitude was computed by integrating the envelope of each signal and computing the average for each scan (20 signals). A Hamming widow of size 7 mm was used to localize the signal from the sample holder and minimize spectral leakage. The power spectrum for each signal was calculated by taking the Fast Fourier Transform and converting to a dB scale. In order to remove the system dependencies on the measurement, the transducer response curve was subtracted from each PA power spectrum. Linear regression was performed on the normalized power spectrum in the 1-8 MHz range. The slope and midband fit (evaluated at 4 MHz) were computed for each PA signal from the linear fit over the normalized PA spectrum. Averages of each of these parameters were then calculated along with the standard deviation of 20 independent measurements. A Shapiro-Wilk test for normality was performed for each spectral parameter from each sample ($W > 0.05$). Once the normality of the data was established, an unpaired t-test was used to

compare the spectral parameters for all hematocrit and aggregation levels to determine statistical significance (denoted by a p-value of 0.05 or less).

3. RESULTS AND DISCUSSION

3.1 Non band-limited modeling of PA spectra

Figure 1(a) demonstrates the 2D spatial organization for a representative sample mimicking NA RBCs at 40% hematocrit. Each circle represents a single RBC. The number of RBCs within the same ROI was varied from 34 for the lowest hematocrit to 842 for the highest hematocrit level. The size of a single RBC, measured by the mean radius of gyration, was 2.13 μm. A representative sample mimicking AG RBCs at 40% hematocrit is shown in figure 1(b). The larger circles enclosing multiple RBCs represent aggregates of the same size. The mean number of clusters was varied between ~55 and ~12 for the lowest to the highest aggregating condition, respectively. The lowest value of the mean radius of gyration was estimated to be 7.57 μm and 15.39 μm for the highest level of aggregation.

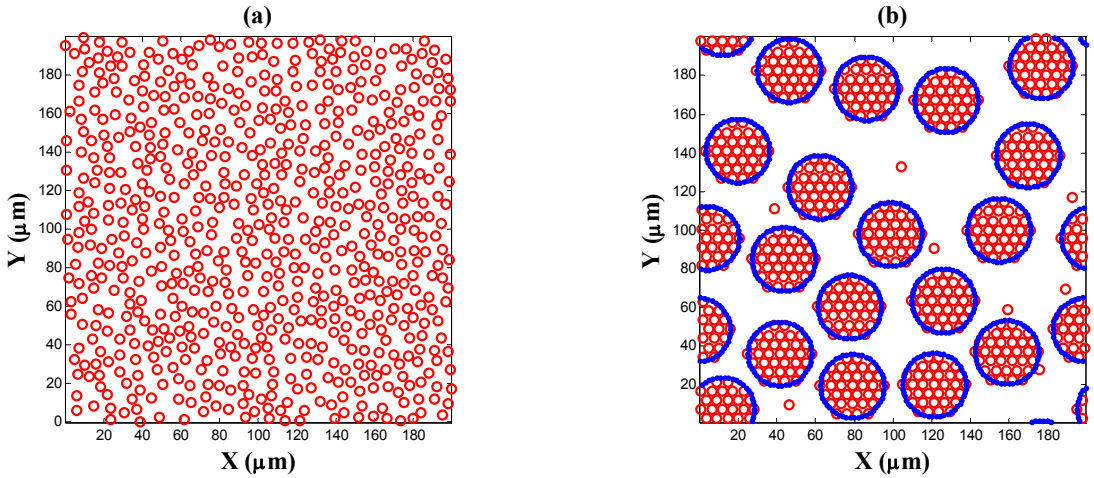

Figure 1. Representative simulated spatial organization for (a) NA RBCs and (b) AG RBCs at 40% hematocrit.

The average spectra of 250 PA signals for NA RBCs from various hematocrit levels are shown in figure 2(a). The spectral power generally increased over all frequencies as the number of RBCs within the ROI increased. The dominant frequency of these signals is related to the size of the individual RBCs[24,26]. This increase also corresponded to a monotonic increase in the PA signal amplitude with increasing hematocrit. Such an increase can be explained by the fact that each individual RBC acts a PA source and increasing their concentration leads to a linear increase in the signal amplitude. This can be inferred by inspection of equation (3): the PA spectral amplitude (and the PA signal) is computed by the linear superposition of the wavelets that each RBC emits when irradiated by a laser source.

The simulated average PA power spectra for AG RBCs are shown in figure 2(b). As the size of the aggregates increased, the spectral power in the low frequency regime (< 30 MHz) also increased. For instance, a 9 dB enhancement was observed at 15 MHz for the 10 μm aggregate compared to the NA case (represented by the 2 μm radius of gyration) at the same hematocrit level. The shift of the dominant frequency towards lower frequencies could be explained by the fact that in the presence of RBC aggregation, the entire aggregate behaves more like a single PA source consisting of multiple RBCs. The origin of the PA signal depends on the heat transfer from the absorbers to the surrounding medium[16]. The relative magnitude of the PA signal of the absorber (i.e. RBC) and of the medium depends on the size of the absorber as well as the size of the illuminated region. The increase in the size of the aggregate along with their spatial organization leads to a reduction of the destructive interference in the low frequency regime thus causing an increase in the signal strength. When RBCs aggregate, the separation distance between adjacent RBCs approaches the thermal diffusion length and it appears as if the PA signal is no longer directly produced by the illuminated absorber but rather the entire aggregate.

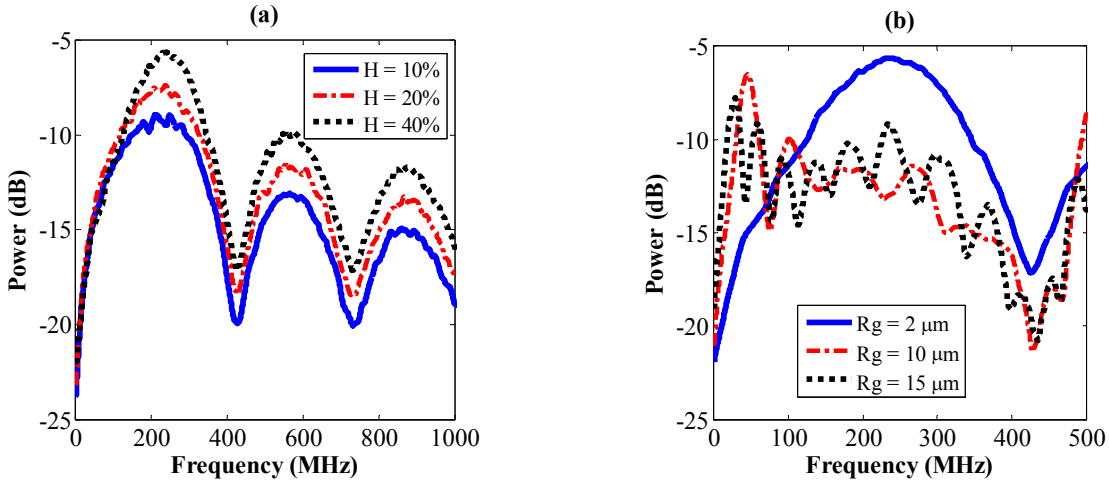

Figure 2. Average, simulated PA power spectra for (a) NA RBCs for three different hematocrits and (b) AG RBCs for three different aggregation levels at 40% hematocrit. The smallest radius of gyration represents the NA RBC case at 40% hematocrit. The frequency scale in (b) only goes up to 500 MHz in order to allow for changes in the low frequency regime to be better visualized.

3.2 Band-limited modeling of PA spectra

The theoretical results for the non band-limited case suggest that PA is capable of distinguishing between the NA and AG blood samples. This is supported from the significant changes observed in the PA spectra of aggregates of varying sizes. However, the results presented above do not take into account the finite nature of the transducers used for the detection of the acoustic waves produced from laser illumination. Since the size of the optical absorber controls the frequency-domain features in PA measurements[26], the bandwidth of the transducer used in the measurement will play a significant role in the detection process. The finite nature of the transducer was modeled as a Gaussian function and was implemented into the model through equation (4).

The spectra that are obtained for 3 transducers with different central frequencies (5, 15 and 55 MHz) and the same -6 dB bandwidth (60%) are shown in figure 3(I) for the same aggregate sizes generated in figure 2(b). The spectral amplitude for both cases is plotted within a 20 dB range. The maximum frequency scale was chosen to be 4 times the central frequency scale of the transducer used. The transducer bandwidth significantly affects the PA signals from the aggregating blood. Therefore the ability of PA techniques to detect changes due to the presence of RBC aggregation is dependent on the transducer receive bandwidth. The 5 MHz (figure 3(b)) and 15 MHz (figure 3 (d)) transducers only demonstrated an increase in the spectral power near the center frequency of the transducer with increasing aggregate size. For the 55 MHz (figure 3(c)) transducer on the other hand, shifts of the spectral power towards lower frequencies were observed as the aggregate size was increased. The difference in the spectral power between NA and AG RBCs at 5, 15 and 55 MHz is plotted in figure 3(II). As the aggregate size increases, significant enhancements of the spectral power were observed for each transducer used. Specifically, enhancements of 5, 8 and 6 dB were observed at 5, 15 and 55 MHz for each transducer used.

The results suggest that frequency-domain analysis of PA signals has the potential to be used as a technique for quantitative tissue characterization, much like quantitative US techniques[19]. The size of the optical absorbers interrogated with PA dictates the dominant frequency content that is detectable with conventional transducers used for PA imaging. Using similar techniques our group has characterized the optical vaporization of perflourocarbon droplets for cancer therapy[27] as well investigated the effects of oxygenation levels of collections of RBCs on the PA signals[28]. In both of these studies, the transducer used for the measurements affected the frequency-domain spectra which are used for the characterization of the samples being investigated. The advantage of PA over US for quantitative tissue characterization lies in the fact that PA allows the use of a variety of optical wavelengths for illuminating the given ROI. This provides the ability to image a variety of physiologically relevant conditions where the oxygenation level can be distinguished through the use of the optically relevant wavelength of illumination[15] in addition to using a variety of exogenous agents designed to target a variety of tissues or anatomies[16].

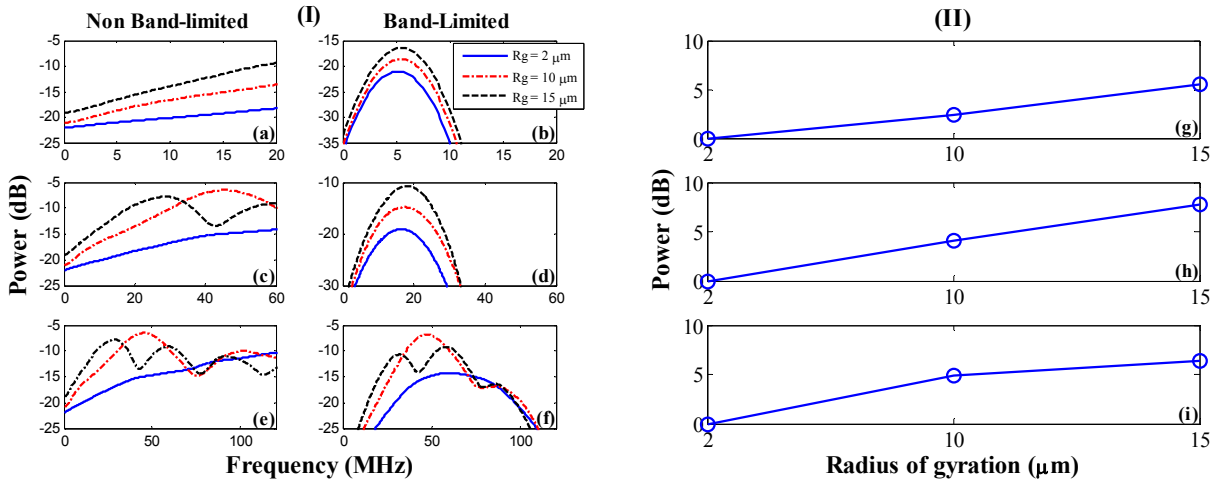

Figure 3. (I) Non band-limited (a, c and e) and band-limited (b, d, and f) average simulated PA spectra for AG RBCs for 3 aggregation levels. The band limited spectra are obtained using transducers with (b) 5 MHz, (d) 15 MHz and (f) 55 MHz center frequency and 60% -6 dB bandwidth. (II) Differences between the spectral powers of NA with AG RBCs at each radius of gyration at (g) 5 MHz, (h) 15 MHz and (i) 55 MHz.

3.3 Experimental PA signals and spectral parameters

The experimental PA signal amplitudes for NA and AG RBCs at various hematocrits levels and Dextran-PBS concentrations are shown in figure 4.

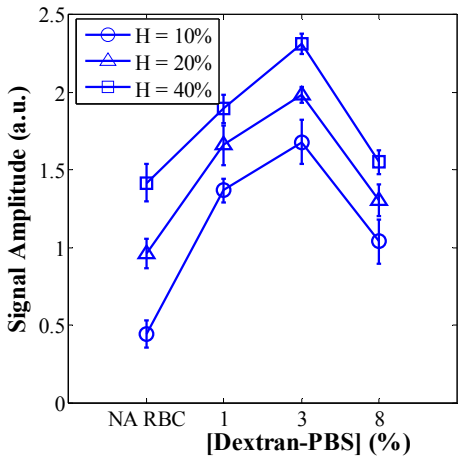

Figure 4: Average PA signal amplitude for all hematocrit levels and Dextran-PBS concentrations used in this study. The error bars indicate the standard deviation for an average of 20 PA measurements.

The amplitude for all of the PA signals at all 3 aggregation levels and all 3 hematocrit levels is statistically significantly higher than the amplitude of the NA case, indicated by a [Dextran-PBS] of 0% (t-test, $p < 0.05$). This suggests that PA imaging and analysis of PA RF signals can be used to differentiate between NA and AG RBCs at various hematocrits and aggregation levels. For the NA case, the PA signal amplitude increased monotonically with increasing hematocrit. This behaviour is also predicted by the band-limited theoretical simulations since the hematocrit is a direct measurement of the concentration of RBCs. Increasing the hematocrit increases the concentration of the PA sources (i.e. RBCs) thus increasing the strength of the PA signal. Other experimental studies have obtained a similar monotonic increase in the PA signal with increasing hematocrit[29]. For the AG cases at 3 different [Dextran-PBS], the PA signal amplitude followed a non-linear trend with increasing [Dextran-PBS]. For all hematocrit levels, the PA signal amplitude was highest for a

[Dextran-PBS] of 3%. This behaviour has also been observed in independent measurements of the degree of aggregation with changing [Dextran-PBS][30,31]. These independent measurements of aggregation are currently the accepted laboratory standard for the assessment of RBC aggregation. The results suggest that PA has the potential of differentiating between different levels of RBC aggregation.

The spectral parameters (midband fit and slope) measured in this study from the normalized power spectra are shown in figure 5. For the NA case, the midband fit (measured in dB, labelled dBr after normalization) increased with increasing hematocrit. This is not surprising as the midband fit is a measure of the normalized power spectra at the middle point of the usable transducer bandwidth. Therefore it is expected that the midband fit as a function of increasing hematocrit exhibit the same behaviour as the PA signal amplitude reported in figure 4. In the AG case, the highest value for the midband fit was observed for the 3% [Dextran-PBS] and at all hematocrit levels and increases are observed with increasing hematocrit. For all the AG samples, there is a statistically significant enhancement in the midband fit compared to the NA cases. The spectral slope (measured in dB/MHz, labelled dBr/MHz after normalization) measured for the same samples shows a statistically significant decrease for all the AG samples compared to the NA ones ($p < 0.05$). Within various aggregating levels, there are no statistically significant differences between the measured spectral slopes. This can be explained by the fact that the PA power spectra do not exhibit any frequency shifts within the transducer bandwidth analyzed. Such behaviour is also predicted by the simulation results which show an enhancement in the power spectra of the measurements with the 5 MHz transducer with no apparent changes in the spectral slope (figure. 2(b)). Moreover, there is no statistically significant change ($p > 0.05$) in the measured spectral slope as a function of hematocrit for both NA and AG samples (figure 5(b)). This again is consistent with theoretical predictions (figure 2(a)).

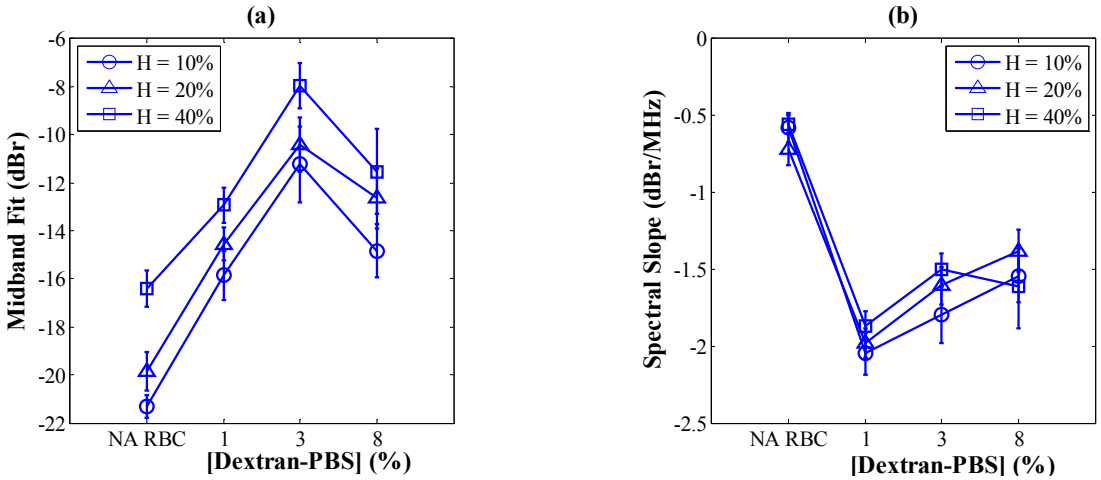

Figure 5: (a) Average midband fit and (b) spectral slope for all hematocrit levels and Dextran-PBS concentrations used in this study. The error bars indicate the standard deviation for 20 PA spectra.

It is important to note that the spectral parameters used in this analysis provide a potential means of assessing the changes that occur during the aggregation process. Taking into account the response of the transducer used for PA measurements removes all system and user dependent settings that make it difficult to compare between experimental conditions. This method of analysis is becoming more commonly used in PA imaging as a means for distinguishing cancerous prostate from normal ones[21] and for monitoring laser heated bovine liver ex-vivo[32]. It is apparent from the theoretical model used in this study that frequency-domain analysis of RF signals in PA provides information about the optical properties of the samples as well as the size of the PA sources[24]. Although the relationship between PA spectral parameters and tissue properties is yet to be determined, the results obtained in this study can be aided in interpretation using what is known from US quantitative tissue characterization (UTC)[20]. In UTC, the spectral slope is an indicator of acoustic scatterer size and shape. An increase in spectral slope corresponds to a decrease in effective scatterer size. In this PA study, a statistically significant decrease in spectral slope in the presence of RBC aggregation is measured; this corresponds to an increase in the effective size of the aggregates as shown in figure 2(b). In UTC, the midband fit is

measure of US backscatter and it depends on acoustic scatterer size and concentration. The increase in midband fit corresponds to an increase in the size of the scatterers and their concentration. In the PA experiments, the increase in the midband fit measured when comparing the NA and AG samples is due to the increase in aggregate size (figure 2(b)). Although inferences of the relationship between these parameters and tissue structures in PA imaging can be made from the established US techniques, more rigorous theoretical framework linking structure of the PA absorbers and the PA RF signals is required. A starting point for determining such relationships could be the design of PA tissue equivalent phantoms with spherical absorbers/scatterers which will allow for measuring of simultaneous PA and US signals. Moreover, since RBCs within the vasculature provide the majority of the PA signals *in-vivo*, modeling the vascular tree is expected to provide insight into this relationship[22,33].

4. CONLCUSIONS

The results presented here demonstrate that PA can be used to detect and characterize the presence of RBC aggregation *in vitro*. The theoretical framework presented here illustrates the ability that PA has to differentiate between NA and AG samples using frequency-domain analysis of the PA signals. Using changes in spectral amplitude and spectral parameters to quantify the degree of aggregation, the experimental results suggest that PA can distinguish between hematocrit and aggregation levels. The techniques adopted in this study propose that PA has the potential of being used as a non-invasive modality for quantitatively characterizing RBC aggregation.

5. ACKNOWLEDGMENTS

The financial support of NSERC, CIHR, CFI and the Canada Research Chairs Program awarded to M. C. Kolios is acknowledged. E. Hysi is supported through the NSERC Alexander Graham Bell Canada Graduate Scholarship program. Jennifer Barry (Comparative Research, Sunnybrook Research Institute) is gratefully acknowledged for her assistance with porcine blood. We are also very thankful to the technical assistance of Arthur Worthington (Ryerson University).

6. REFERENCES

[1] Baskurt, O. K. and Meiselman, H. J., "Blood rheology and hemodynamics," Semin. Thromb. Hemost. 29(5), 435-450 (2003).
[2] Holley, L., Woodland, N., Hung W. T., Cordatos, K. and Reuben, A., "Influence of fibrinogen and haematocrit on erythrocyte sedimentation kinetics," Biorheology 36, 287-297 (1999).
[3] Nash, G. B., Wenby, R. B., Sowemimo-Coker, S. O. and Meiselman, H. J., "Influence of cellular properties on red cell aggregation," Clin. Hemorheol. 7, 93-108 (1987).
[4] Shung, K. K. and Thieme, G. A., [Biological Tissue as Ultrasonic Scattering Media in Ultrasonic Scattering in Biological Tissue], CRC Press, Boca Raton, 57-59 (1993).
[5] Johnson, P. C., Bishop, J. J., Popel, S. and Intaglietta M., "Effects of red cell aggregation on the venous microcirculation" Biorheology 36, 457-460 (1999).
[6] Cloutier, G., Zimmer, A., Yu, F. and Chiasson, J. L., "Increased shear rate resistance and fastest kinetics of erythrocyte aggregation in diabetes measured with ultrasound," Diabetes Care 31(7), 1400-1402 (2008).
[7] Yu, F. T. H., Armstrong, J. K., Tripette, J., Meiselman, H. J. and Cloutier, G., "A local increase in red blood cell aggregation can trigger deep vein thrombosis: evidence based on quantitative cellular ultrasound imaging," J. Thromb. Haemost. 9, 481-488 (2011).
[8] Meiselman, H. J., "Red blood cell aggregation: 45 years being curious," Biorheology 46, 1-9 (2009).
[9] Baskurt, O. K., Temiz, A. and Meiselman, H. J., "Red blood cell aggregation in experimental sepsis," J. Lab. Clin. Med. 130(2), 183-190 (1997).
[10] Lee, S. J., Ha, H. and Nam, K., "Measurement of red blood cell aggregation using X-ray phase contrast imaging," Opt. Express 18(25), 26052-26061 (2010).
[11] Xu, X., Yu, L. and Chen, Z., "Velocity variation assessment of red blood cell aggregation with spectral domain doppler optical coherence tomography," Ann. Biomed. Eng. 38(10), 3210-3217 (2010).
[12] Franceschini, E., Yu, F. T. H., Destrempes, F. and Cloutier, G., "Ultrasound characterization of red blood cell aggregation with intervening attenuating tissue mimicking phantoms," J. Acoust. Soc. Am. 127(2), 1104-1115 (2010).
[13] Wang, L. V., "Prospects of photoacoustic tomography," Med. Phys. 35(12), 5758-2767 (2008).

[14] Emelianov, S. Y., Li, P. and O'Donnell, M., "Photoacoustics for molecular imaging and therapy," Phys. Today 62(5), 34-39 (2009).
[15] Wang, X., Xie, X., Ku, G., Wang, L. V. and Stoica, G., "Noninvasive imaging of hemoglobin concentration and oxygenation in rat brain using high-resolution photoacoustic tomography," J. Biomed. Opt. 11(2), 024015-1-9 (2006).
[16] Chen, Y., Frey, W., Kim, S., Kruizinga, P., Homan, K. and Emelianov S., "Silica-coated gold nanorods as photoacoustic signal nanoamplifiers," Nano Lett. 11, 348-354 (2011).
[17] Hysi, E., Saha, R. K. and Kolios, M. C., "Characterization of red blood cell aggregation with photoacoustics: a theoretical and experimental study," Proc. IEEE IUS, in press (2011).
[18] Lizzi, F. L., Ostromogilsky, M., Feleppa, E. J., Rorke, M. C. and Yaremko, M. M., "Relationship of ultrasonic parameters to features of tissue microstructure," IEEE T. Ultrason. Ferr. 33(3), 319-329 (1987).
[19] Kolios, M. C. and Czarnota, G. J., "Potential use of ultrasound for the detection of cell changes in cancer treatment," Future Oncol. 5(10), 1527-1532 (2009).
[20] Lizzi, F. L., Greenbaum, M., Feleppa, E. J., Elbaum, M. and Coleman, D. J., "Theoretical framework for spectrum analysis in ultrasonic tissue characterization," J. Acoust. Soc. Am. 73(4), 1366-1373 (1983).
[21] Kumon, R. E., Deng, C. X. and Wang, X., "Frequency-domain analysis of photoacoustic imaging data from prostate adenocarcinoma tumors in a murine model," Ultrasound Med. Biol. 37(5), 834-839 (2011).
[22] Zalev, J. and Kolios, M. C., "Detecting abnormal vasculature from photoacoustic signals using wavelet-packet features," Proc. SPIE 7899, 78992M-1-15 (2011).
[23] Saha, R. K. and Kolios, M. C., "A simulation study on photoacoustic signals from red blood cells," J. Acoust. Soc. Am. 129(5), 2395-2943 (2011).
[24] Diebold G. J., [Photoacoustic Monopole Radiation: Waves from Objects with Symetry in One, Two and Three Dimensions in Photoacoustic Imaging and Spectroscopy], CRC Press, Boca Raton, 3-17 (2009).
[25] Szabo, T. J., [Diagnostic Imaging: Inside Out], Elsevier Academic Press, San Diego, 97-135 (2004).
[26] Rui, M., Bost, W., Weiss, E. C., Lemor, R. and Kolios, M. C., "Photoacoustic microscopy and spectroscopy of individual red blood cells," OSA Opt. & Photo. Congress BIOMED/DH, BSuD93 (2010).
[27] Strohm, E., Rui, M., Gorelikov, I., Matsuura, N. and Kolios, M. C., "Vaporization of perfluorocarbon droplets using optical irradiation," Biomed. Opt. Express 2(6), 1432-1442 (2011).
[28] Saha, R. K. and Kolios, M. C., "Effects of erythrocyte oxygenation on optoacoustic signals," J. Biomed. Opt. 16(11), 115003-1-9 (2011).
[29] Karpiouk, A. B., Aglyamov, S. R., Mallidi, S., Shah, J., Scott, W. G., Rubin, J. M. and Emelianov, S. Y., "Combined ultrasound and photoacoustic imaging to detect and stage deep vein thrombosis: phantom and ex vivo studies," J. Biomed. Opt. 13(5), 054061-1-1-8 (2008).
[30] Baskurt, O. K., Farley, R. A. and Meiselman, H. J., "Erythrocyte aggregation tendency and cellular properties in horse, human and rat: a comparative study," Am. J. Physiol. Heart Circ. Physiol. 273, H2604-H2612 (1997).
[31] Armstrong, J. K., Wenby, R. B., Meiselman, H. J. and Fisher, T. C., "The hydrodynamic radii of macromolecules and their effect on RBC aggregation," Biophys. J. 87, 4259-4270 (2004).
[32] Patterson, M. P., Riley, C. P., Kolios, M. C. and Whelan, W. M., "Optoacoustic signal amplitude and frequency spectrum analysis laser heated bovine liver ex-vivo," Proc. IEEE IUS, in press (2011).
[33] Zalev, J., "Detection and monitoring for cancer and abnormal vasculature by photoacoustic signal characterization of structural morphology," M.Sc. thesis, Ryerson Univ., 2010.